Model Building and Experimental Validation for Regeneration of Perpendicular Vibration by In-Wheel Motor

Haru Ichikawa[1], Takumi Ueno[2], Osamu Shimizu[3] and Hiroshi Fujimoto[4]

***Abstract*— Traditional hydraulic dampers dissipate the energy of perpendicular vibration as heat to improve ride comfort. Therefore, numerous studies have been conducted to recover the energy as electricity instead of wasting it. Most of this studies involve converting perpendicular vibration energy into rotational kinetic energy, which is regenerated as electric power using motors. However, this study proposes a novel idea of regenerating perpendicular vibration energy in electric vehicles (EVs) using drive motors mounted inside wheels. This approach aims to focus on the perpendicular forces generated by the driving force owing to the suspension geometry and recover vibration energy that is potentially converted into rotational energy owing to the structure. In this study, a new model is proposed that considers the torque disturbance owing to the vibration. Through simulations and experiments, the drive motors were confirmed to recover the vibration energy, and a novel loss separation method was proposed. To analyze the effectiveness, a suspension force regeneration control was applied. Analysis of the experimental results demonstrated that the suspension force can be regenerated as electric power by drive motors.**

I. Introduction

The suspension of vehicles is essential for preventing perpendicular vibrations by disturbances, such as road conditions and vehicle motions. Most suspension systems consist of springs and viscous shock absorbers. Currently, many vehicles use hydraulic passive dampers as shock absorbers, dissipating the vibration energy into the air as heat and improving ride comfort and driving stability. In general, $100\,\mathrm{W}$–$400\,\mathrm{W}$ of power is dissipated by four traditional dampers when a middle-sized vehicle is running on an average road at approximately $100\,\mathrm{km/h}$ [1]. Our research proposes a new approach for EVs, in which vibration energy is recovered by the drive motor.

Several studies have been conducted to recover the vibration energy, which is dissipated initially as heat by the traditional damper [2]–[6]. In [2], a two-leg mechanism is used to regenerate the vibration energy. In [3], multiple controlled transducers are used, which can widely adjust the damper coefficient. In [4], an experimental rig is developed and demonstrated regenerative power. In [5], the hydraulic electromagnetic energy-harvesting shock absorber is designed. In [6], the self-powered suspension using a ball screw is proposed. A common point in these studies on the regenerative damper is the development of a mechanism to convert the perpendicular vibration into rotational motion, and coupled longitudinal and perpendicular motions that occur when the suspensions are mounted on vehicles are not considered.

Generally, semi-active and active dampers, which can change the hydraulic pressure of the damper depending on the road surface and driving conditions, can provide better ride comfort than passive dampers. Several studies have focused on actively utilizing the perpendicular forces that the drive motors can generate to suppress vibrations without the additional structures to improve ride comfort [7]–[9]. In [7], the perpendicular forces are used to suppress the vibration at $4\,\mathrm{Hz}$–$8\,\mathrm{Hz}$, which is uncomfortable for passengers. In [8], the roll motion of the vehicle is suppressed by controlling the perpendicular forces. Both studies are applied to in-wheel motor (IWM) EVs, in which each motor is mounted on each wheel, and research on them and their control has been active recently [10]–[12]. In [9], a method to determine the driving force input that minimizes the dissipation power caused by tire slip, considering the perpendicular forces, to achieve the desired 6-DOF motion is proposed. As aforementioned, the perpendicular force can be directly controlled by the drive motor torque, and the behaviour on the springs can be controlled as in active suspension. The generation of perpendicular forces can be explained by force balancing, and torque disturbances should occur when the suspension stroke changes owing to road surface disturbances. However, the torque disturbance is not considered in these studies.

Inspired by research into conventional regenerative dampers and vibration control with drive motors, we propose a novel model of regenerating vibration energy. Our research shows that some of the energy from perpendicular vibration can be regenerated by the drive motor without additional mechanisms. We established the method of energy analysis, encompassing the influence of perpendicular vibrations, by demonstrating qualitative consistency between simulations and experimental results. Based on the loss separation, the suspension force regeneration control was applied. The experimental result demonstrated that perpendicular vibration can be regenerated as electric power by the drive motor.

II. Vehicle Dynamics Model

A. Vehicle motion model

This subsection describes a model of the four-wheel drive IWM-EV. Because only straight driving is considered in this paper, the left and right driving-braking forces are equal. Therefore, the longitudinal motion of the vehicle and wheel

[1]Haru Ichikawa, Takumi Ueno, Osamu Shimizu and Hiroshi Fujimoto are with Graduate School of Frontier Science, The University of Tokyo, 5-1-5, Kashiwanoha, Kashiwa, Chiba, 277-8561, Japan ichikawa.haru23@ae.k.u-tokyo.ac.jp

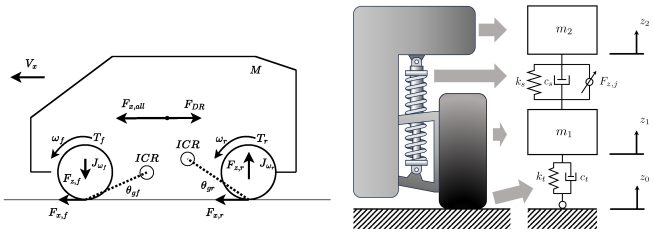

(a) (b)

Fig. 1. Vehicle motion models. (a)Coupled longitudinal and perpendicular motion. (b)Quater car vibration model.

rotational motions are expressed as

$$M\dot{V}_x = F_{x,all} - F_{DR} = 2\sum_{j=f,r} F_{x,j} - F_{DR}, \tag{1}$$

$$J_{\omega_j}\dot{\omega}_j = T_j - rF_{x,j} + M_{s,sus,j}, \tag{2}$$

where M is the vehicle mass, V_x is the vehicle chassis velocity, $F_{x,all}$ is the total driving-braking force, F_{DR} is the driving resistance, $F_{x,j}$ is the driving-braking force of each wheel, J_{ω_j} is the wheel inertia, ω_j is the wheel angular velocity, T_j is the motor torque, r is the wheel radius, and $M_{s,sus,j}$ is the torque disturbance from the suspension forces, respectively. The subscript j represents f or r (f represents front, and r represents rear).

The slip ratio is defined as

$$\lambda_j = \frac{r\omega_j - V_x}{\max(r\omega_j, V_x, \epsilon)}, \tag{3}$$

where ϵ is a small constant to avoid zero division. The slip ratio λ_j is expressed as the function of the road friction coefficient μ_j [13]. Therefore, the driving-braking forces are expressed as $F_{x,j} = \mu_j(\lambda_j)N_j$, where N_j is the tire load.

B. Coupled longitudinal and perpendicular motion

When the driving-braking forces are generated, pitch moments are generated around the CoG. To suppress the pitch moments, a mechanism called "anti-dive geometry" is designed into the suspension and chassis [14]. Because the suspension is connected to the vehicle body via multiple arms, there are instantaneous centers of rotations (ICR), as illustrated in Fig. 1 (a). When the driving-braking forces generate moments around the ICRs, the perpendicular forces $F_{z,j}$ are generated as the reaction from the moments around the ICRs to the vehicle body, which are expressed as

$$F_{z,f} = -F_{x,f}\tan\theta_{gf}, \tag{4}$$

$$F_{z,r} = F_{x,r}\tan\theta_{gr}, \tag{5}$$

where θ_{gj} is the ICR elevation angle from the point of contact between the wheel and the ground.

When the vehicle vibrates owing to the road disturbance and other factors, such as the road slope and vehicle motion, the suspension stroke changes, and suspension force $F_{z,sus,j}$ is generated. The suspension force generates a moment around the ICR, and the motor regenerates the moment $M_{s,sus,j}$ as a torque disturbance to maintain force balance, which is expressed as

$$M_{s,sus,f} = -F_{z,sus,f}\cdot l_{gf}\cos\theta_{gf}, \tag{6}$$

$$M_{s,sus,r} = F_{z,sus,r}\cdot l_{gr}\cos\theta_{gr}, \tag{7}$$

where l_{gf} and l_{gr} are the distances from the front and rear wheel ground points to the ICRs, respectively.

Fig. 1 (b) illustrates the quarter car vibration model. This model consists of the quarter sprung mass, quarter unsprung mass, suspension, and wheel. The perpendicular motion is expressed as

$$\begin{aligned} m_2\ddot{z}_2 =& -F_{z,sus,j} + F_{z,j} \\ =& -k_s(z_2 - z_1) - c_s(\dot{z}_2 - \dot{z}_1) + F_{z,j}, \end{aligned} \tag{8}$$

$$\begin{aligned} m_1\ddot{z}_1 =& k_s(z_2 - z_1) + c_s(\dot{z}_2 - \dot{z}_1) \\ & - k_t(z_1 - z_0) - c_t(\dot{z}_1 - \dot{z}_0) - F_{z,j}, \end{aligned} \tag{9}$$

where k_s and k_t are the stiffness of the spring and tire, c_s and c_t are the damping coefficient of the spring and tire, and z_2, z_1, and z_0 are the displacements of the sprung mass, unsprung mass, and road, respectively.

III. Inverter input power loss Separation

This section shows a method to separate the inverter input power loss based on the motor and vehicle motion model. By neglecting the inverter loss and mechanical loss of the motor, the inverter input power P_{in} is expressed as

$$P_{\text{in}} = P_c + P_i + P_{\text{out}}, \tag{10}$$

where P_c is the sum of the copper loss of each motor, P_i is the sum of the iron loss of each motor, and P_{out} is the sum of the mechanical output of each motor.

Assuming that the *q*-axis current is large compared to the *d*-axis current, the copper loss, iron loss, and mechanical output of each motor are calculated as follows [15] [16]

$$P_c = 2\sum_{j=f,r} R_j i_{qj}^2 = 2\sum_{j=f,r}\frac{R_j T_j^2}{K_{tj}^2}, \tag{11}$$

$$P_i = \sum_{j=f,r}\frac{(p_{nj}\omega_j)^2}{R_{cj}}\left\{\left(\frac{L_{qj}T_j}{K_{tj}}\right)^2 + \Psi_j^2\right\}, \tag{12}$$

$$P_{\text{out}} = 2\sum_{j=f,r}\omega_j T_j, \tag{13}$$

where R_j is the winding resistance of the motor, i_{qj} is the q-axis current, K_{tj} is the torque coefficient of the motor, R_{cj} is the iron loss resistance, L_{qj} is q-axis inductance, Ψ_j is the interlinkage magnetic flux, and p_{nj} is the number of pole pairs, respectively.

In the following discussion, P_{out} is further separated based on (2). Assuming that the slip ratio of each wheel is sufficiently small, the vehicle speed is approximated as $V_x = r\omega_j$. Moreover, we only consider the rear-wheel drive

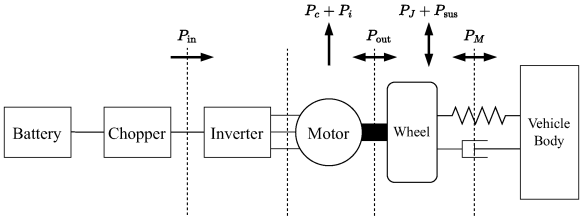

Fig. 2. The energy flow. In the figure, $P_{\rm sus} = P_{\rm sp} + P_{\rm dam}$.

system for simplicity.

$$\begin{aligned}\omega_r T_r &= r\omega_r F_{x,r} + J_{\omega_r}\omega_r\dot{\omega}_r - \omega_r M_{s,sus,r} \\ &= V_x\left(\frac{M\dot{V}_x}{2} + \frac{1}{2}F_{DR}\right) + J_{\omega_r}\omega_r\dot{\omega}_r - \omega_r M_{s,sus,r} \\ &= \frac{1}{2}\frac{d}{dt}\left(\frac{1}{2}MV_x^2\right) + \frac{d}{dt}\left(\frac{1}{2}J_{\omega_r}\omega_r^2\right) \\ &\quad + \frac{1}{2}F_{DR}V_x - \omega_r M_{s,sus,r}. \end{aligned} \tag{14}$$

By substituting (14) into (10), $P_{\rm in}$ is separated as

$$P_{\rm in} = P_c + P_i + P_M + P_J + P_{DR} + P_{\rm sp} + P_{\rm dam}, \tag{15}$$

where P_M is the power stored as kinetic energy of the vehicle mass, and P_J is the power stored as rotational energy of each wheel, respectively. P_{DR}, $P_{\rm sp}$, and $P_{\rm dam}$ are the loss by the driving resistance, suspension force, and suspension damper, respectively. For the rear-wheel drive system, each power is expressed as

$$P_c = \frac{2R_r T_r^2}{K_{tr}^2}, \tag{16}$$

$$P_i = \frac{2\left(p_{nr}\omega_r\right)^2}{R_{cr}}\left\{\left(\frac{L_{qr}T_r}{K_{tr}}\right)^2 + \Psi_r^2\right\}, \tag{17}$$

$$P_M = \frac{d}{dt}\left(\frac{1}{2}MV_x^2\right), \tag{18}$$

$$P_J = 2\frac{d}{dt}\left(\frac{1}{2}J_{\omega_r}\omega_r^2\right), \tag{19}$$

$$P_{DR} = F_{DR}V_x, \tag{20}$$

$$P_{\rm sp} = -2k_s(z_2 - z_1)\omega_r l_{gr}\cos\theta_{gr}, \tag{21}$$

$$P_{\rm dam} = -2c_s(\dot{z}_2 - \dot{z}_1)\omega_r l_{gr}\cos\theta_{gr}. \tag{22}$$

(15) shows that the suspension forces could be working toward the motor's rotation. Additionally, a portion of the power is dissipated by the damper. To reduce the power dissipated, $P_{\rm dam}$ can be made smaller. Note that this loss separation considers cases where the motor fully compensates for torque disturbances caused by suspension forces. The aforementioned concept is represented in Fig. 2.

IV. Evaluation

To validate the proposed model, this section analyzes the powers when the vehicle vibrates while driving at the constant velocity in simulations and experiments. Fig. 3 illustrates the experimental vehicle, FPEV-5, developed by our research group. The vehicle has a rear-wheel drive system

TABLE I
Vehicle Specifications.

Symbol	Value
M	1174 kg
J_{ω_r}	1.24 kg m^2
l_f, l_r	1.44 m, 1.11 m
l	2.55 m
h_g	0.51 m
θ_{gr}	0.222 rad
l_{gr}	2.451 m

TABLE II
IWM Specifications.

Symbol	Value
r	0.294 m
R_r	0.235 Ω
K_{tr}	3.32 Nm/A
R'_{cr}	0.21 Ωs/rad
L_{qr}	1.44 mH
Ψ_r	0.237 Wb
p_{nr}	14

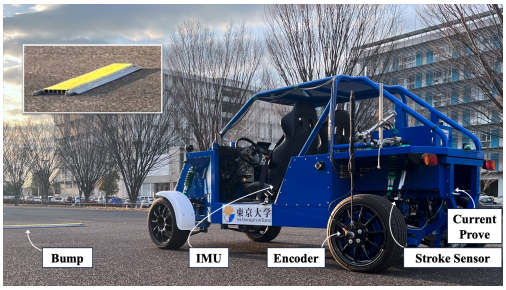

Fig. 3. Experimental vehicle FPEV-5. The bump is trapezoidal in shape with the top base of 20 cm, the bottom of 40 cm, and the height of 5 cm.

with two IWMs and is equipped with a dSPACE DS1007 processor board. The vehicle is equipped with a double wishbone suspensions, and the θ_{gr} is obtained from the CAD data of the blueprints. The suspension is commercially available, and the damping can be adjusted in 16 steps. The vehicle specifications and the motor parameters are summarized in TABLE I and II. Simulations were performed using MATLAB/Simulink based on the experimental vehicle.

In simulations and experiments, driving resistance F_{DR}, consisting of rolling friction and air resistance, which is generated when the vehicle is in motion, is calculated as

$$F_{DR}(V_x) = \mu_0 Mg + \frac{4}{r^2}B_r V_x + \frac{1}{2}\rho C_d A V_x^2, \tag{23}$$

where μ_0 is the rolling friction coefficient, B_r is the viscous damping coefficient, ρ is the air density, C_d is the drag coefficient, and A is the frontal projected area, respectively.

A. Simulation Result

The velocity control system was designed to validate the model. A proportional-integral (PI) velocity controller was designed through the pole placement for the following plant.

$$\frac{\omega_r}{T_r} = \frac{1}{\left(J_{\omega_r} + r^2 M\left(1 - \lambda_{rn}\right)\right)s}. \tag{24}$$

The pole was set to $-0.3\,{\rm rad/s}$. The nominal slip ratio λ_{rn} was fixed as 0.05, assuming the experiment was on a dry, non-slippery road surface.

In the simulation, the rear suspension was compressed while the vehicle ran at a constant velocity of $10\,{\rm km/h}$ by the velocity control. This confirms that torque disturbances are generated and suppressed by the velocity control. The power was analyzed from the moment when the suspension stroke was reduced to the initial state until the vibration converged.

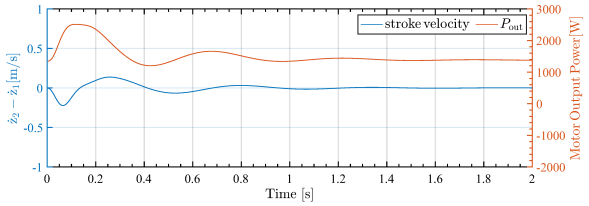

Fig. 4. Simulation result of the relationship between suspension stroke velocity and motor output power.

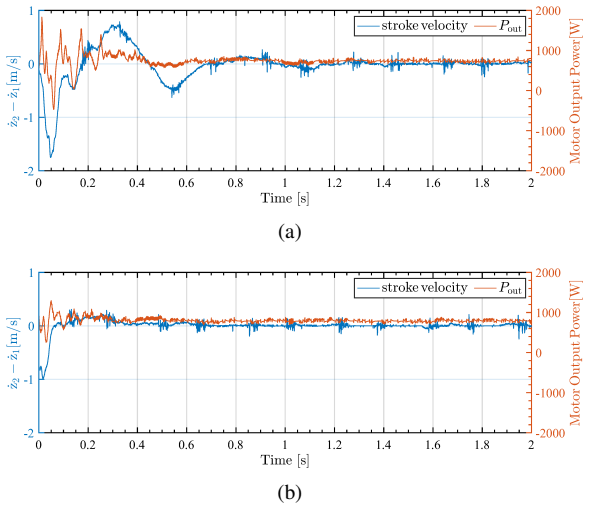

Fig. 5. Experimental result of the relationship between suspension stroke velocity and motor output power. (a)Low damping. (b)High damping.

Fig. 4 illustrates the suspension stroke velocity and motor output power. Crucially, the torque disturbance occurs at the same frequency as the force generated by the suspension, and the velocity control compensates for that, resulting in the motor output oscillating at the same frequency.

B. Experimental Setting

In the experiment, the velocity control is applied, with the vehicle going over a 5 cm high trapezoidal bump at the constant velocity of 10 km/h. Comparative analysis of the rear suspension stroke, P_{out} and P_{in} was conducted after exceeding the bump. The suspension stroke change is obtained from the stroke sensor, and the wheel velocity is obtained from an optical encoder with 12-bit resolution. P_{in} was calculated using current probes and voltage sensors.

C. Experimental Result

Fig. 5 illustrates the suspension stroke velocity and motor output power when damping is low and high. Note that at $t = 0$ the EV lands on the ground. It can be observed that the motor output oscillates in response to changes in suspension stroke, although only the velocity control is used to control movement in the longitudinal direction.

The results of fast Fourier transform (FFT) for the suspension stroke and P_{in} are shown in Fig. 6. The solid line shows the results at low damping and the dashed line at high damping. In Fig. 6, the solid line shows the peak around 2 Hz in the suspension stroke plot, the resonance of the spring,

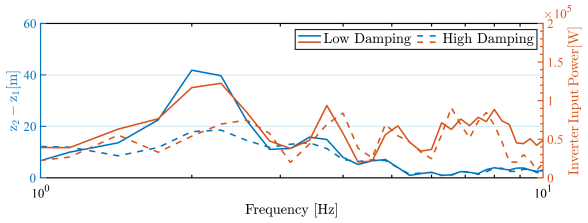

Fig. 6. FFT result of the suspension stroke and the inverter input power.

and the peak in P_{in} is near 2 Hz [17]. However, the dashed line shows that the resonance of the spring decrease when the damping is high, and peak in P_{in} near 2 Hz decrese accordingly. This shows that the suspension stroke and P_{in} are correlated.

The aforementioned results qualitatively showed the same trend as the simulation and demonstrated the validity of the proposed model. The torque disturbance is compensated by the velocity control to ensure that P_{out} is similar to when vibration control is used, although only the longitudinal motion is controlled. This shows the possibility of regenerating perpendicular motions with only the drive motor.

V. Application to Suspension Force Regeneration Control

Based on the validated model, vibration suppression control is described as the regeneration of suspension forces. Theoretical analysis that resembles the suspension force regeneration is performed by separating the loss of P_{in} when vibration suppression control is applied.

A. Damping coefficient control

Active suspensions can control the damping coefficient of the dampers; however, in this study, the IWMs assumes an equivalent role. The perpendicular force is expressed as

$$F_{z,r} = -\alpha c_s(\dot{z}_2 - \dot{z}_1), \tag{25}$$

where α is the control gain. If the perpendicular force expressed as (25) is generated, the apparent damping coefficient changes to $(1-\alpha)c_s$. If it is assumed that the tires do not lift off the ground ($\dot{z}_1 = 0$), (25) is equivalent to the skyhook damper control [18]. The torque to generate the desired perpendicular force, T_{vib}, is calculated as

$$T_{vib} = \frac{rF_{z,r}}{\tan\theta_{gr}} = -\alpha\frac{rc_s(\dot{z}_2 - \dot{z}_1)}{\tan\theta_{gr}}. \tag{26}$$

Vibration suppression control is applied to quickly converge the perpendicular vibration on the spring and reduce the amplitude of the perpendicular vibration. However, the common point is that it generates forces in a direction that counteracts the perpendicular forces caused by changes in suspension stroke, the regeneration of suspension forces. Consequently, the skyhook damper control regenerates the force generated by the damper out of the suspension force and can control P_{dam} in (15). However, the force generated by the spring cannot be regenerated. Therefore, P_{sp} in (15) is zero, and the force is not regenerated by the motor, but decomposed into longitudinal forces and other forces.

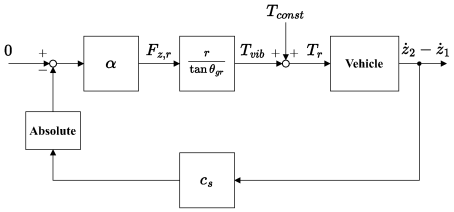

Fig. 7. Control system for regenerating the suspension forces (Case 3).

B. Experimental Setting

In the experiment, the velocity control was applied to enter the bump at a constant velocity of $10\,\mathrm{km/h}$. When the rear wheels came off the bump, the velocity control was stopped and switched to the suspension force regeneration control. To evaluate the effectiveness, the following three cases were performed after the switching.

- Case 1: $T_r = T_{const}$
- Case 2: $T_r = -\alpha \dfrac{r c_s (\dot{z}_2 - \dot{z}_1)}{\tan\theta_{gr}} + T_{const}$
- Case 3: $T_r = -\alpha \dfrac{r c_s |\dot{z}_2 - \dot{z}_1|}{\tan\theta_{gr}} + T_{const}$

In the experiment, $\alpha = 0.15$, $T_{const} = 50\,\mathrm{Nm}$, and $c_s = 2000\,\mathrm{Ns/m}$. We introduce a constant torque, the value of which is approximately equal to some driving resistance. Cases 2 and 3 regenerate the force from the dampers out of the suspension force; however, Case 2 is a normal skyhook damper control, whereas Case 3 is the skyhook damper control that feeds back the absolute value of the suspension stroke velocity. Based on the drive motor, one side of the perpendicular force is regenerative, while the other is a loss. Therefore, in Case 3, normal skyhook damper control is performed in the regenerative direction from the drive motor's point of view. However, the force in that direction is increased in the loss direction. A block diagram of the whole control system is shown in Fig. 7.

C. Experimental Validation

The experimental results are shown in Fig. 8. When the rear wheels come off the bump, and the control is switched and defined as $0\,\mathrm{s}$. Fig. 8 is showing the loss separations of P_{in}, P_{out}, and W_{in}. The integrated value of each power calculated as in the following equation.

$$W_y = \int_0^{0.7} P_y \, dt \quad (y = \mathrm{in}, c, i, M, J, DR, \mathrm{sus}). \tag{27}$$

Here, P_{sus} is calculated as $P_{\mathrm{sus}} = P_{\mathrm{sp}} + P_{\mathrm{dam}}$. The integral section is set at the section where the vibration owing to bumps is large. Fig. 8 shows that P_{in} and P_{out} loss separation is successful in the time domain. When a constant torque command is given, P_{sp} and P_{dam} are set to zero because neither the spring nor the damper force can be regenerated. In Cases 2 and 3, P_{dam} was considered. Thus, loss separation of motor output was performed.

In Fig. 8 (i), W_M is smaller than the others, indicating that the motor recovers kinetic energy through regenerative braking. However, W_{sus} also accounts for a large proportion of the motor output W_{out}, and regenerating the vibration caused by the damper can reduce the motor output and inverter input energy. To consider excluding the difference of the change in kinetic energy, $W_{\mathrm{in}} - W_M$ is shown in the figure. The relationship of $W_{\mathrm{in}} - W_M$ is also the same as that of W_{in}, and it is understood that the difference is owing to copper loss W_c and W_{sus}.

In Fig. 8 (e)(f) the power from the suspension P_{sus} accounts for approximately $50\,\%$ of the motor output power P_{out}. Therefore, it can be understood that P_{in} changes significantly owing to vibration energy when vibration suppression control is applied, and the potential for vibration energy regeneration by the drive motor is large.

D. Consideration on other road surfaces

The amount of vibration energy that can be regenerated is determined by changes in suspension stroke, suspension mounting and the torque limit of the motor, thus it can be assumed that there is an energy gain from driving with vibration suppression control on ordinary roads.

According to ISO standards, road surface roughness can be classified into eight classes, from A to H, according to power spectral density. Using the road roughness coefficients derived from the power spectral density, the road surface displacement can be expressed by a stationary Gaussian stochastic process as [3]

$$\dot{z}_0(t) = -2\pi f_0 z_0(t) + 2\pi\sqrt{G_0 V_x} w(t), \tag{28}$$

where f_0 is the lower cut-off frequency, G_0 is the road roughness coefficient, and $w(t)$ is random white noise whose power is equal to 1.

The theoretical regenerative power available to the EV runs at constant velocity $10\,\mathrm{m/s}$ on the regular road classB, when a road displacement expressed in (28) is input to the vehicle, is shown in the Fig. 9. The ICR elevation angle of the experimental vehicle is designed to be smaller than that of a standard vehicle, implying that the regenerative vibration energy is larger, but still generates around $5000\,\mathrm{W}$ instantaneously. Although it is difficult to regenerate all of this through the motor's torque limit, it is clear that the vibration energy owing to the suspension is generated in a non-negligible way even during normal driving.

VI. Conclusion

In this study, a model is proposed in which suspension forces work in the direction of rotation of the drive motor in the IWM-EV by considering the longitudinal and perpendicular motions coupled through the suspension. The model was validated through real vehicle experiments, which showed qualitatively the same experimental results as the simulation.

From the proposed model, the analysis method for inverter input power considering perpendicular vibration was established and demonstrated in experiments of the suspension force regeneration control. The experiments with the suspension force regeneration control showed that the inverter input power varied depending on the control method used,

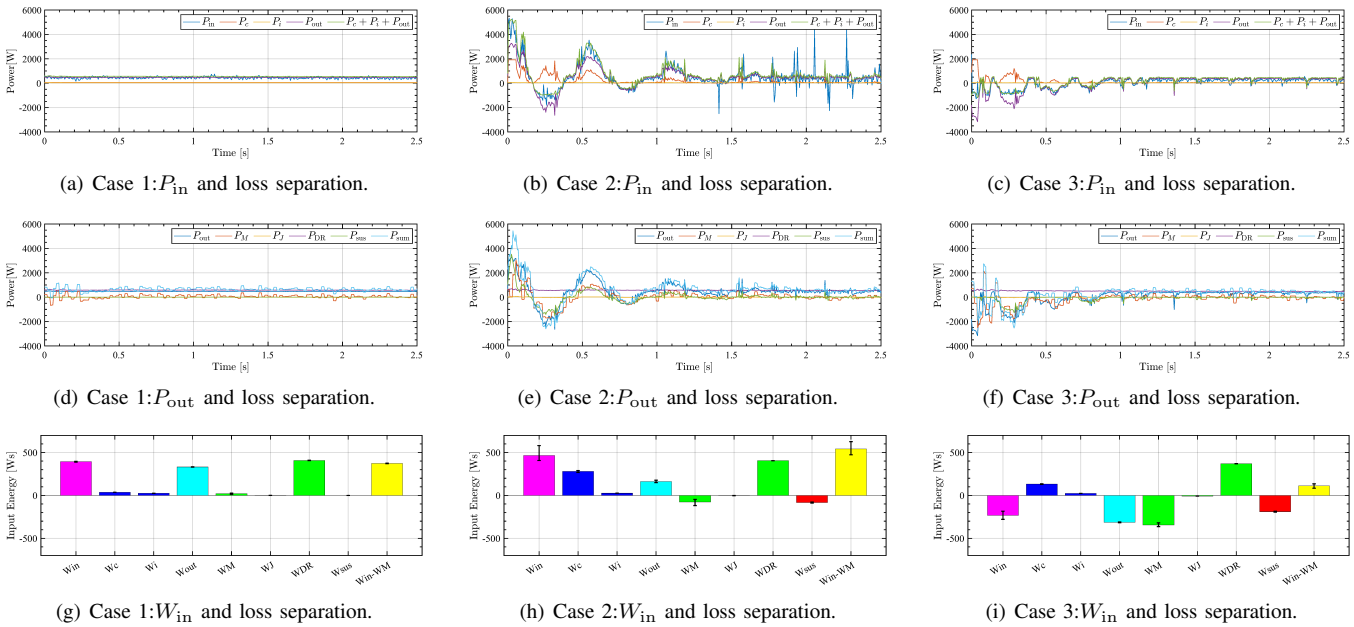

(a) Case 1:P_{in} and loss separation. (b) Case 2:P_{in} and loss separation. (c) Case 3:P_{in} and loss separation.

(d) Case 1:P_{out} and loss separation. (e) Case 2:P_{out} and loss separation. (f) Case 3:P_{out} and loss separation.

(g) Case 1:W_{in} and loss separation. (h) Case 2:W_{in} and loss separation. (i) Case 3:W_{in} and loss separation.

Fig. 8. Experimental results. In the figure, $P_{\mathrm{sum}} = P_M + P_J + P_R + P_{\mathrm{sus}}$

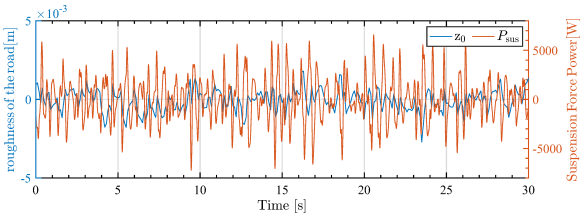

Fig. 9. Relationship between roughness of the road and the vibration energy that can in principle be regenerated under the road classB.

and that the suspension force work, the vibration energy, made a significant contribution to the variation.

Future prospects include the proposal of a vibration suppression control method using IWM, which has advantages in terms of energy, based on the model and analysis method proposed in this paper.

REFERENCES

[1] L. Zuo, P. Zhang, "Energy Harvesting, Ride Comfort, and Road Handling of Regenerative Vehicle Suspensions," *Journal of Vibration and Acoustics*, vol. 135, no. 1, 2013.

[2] A. Maravandi and M. Moallem, "Regenerative Shock Absorber Using a Two-Leg Motion Conversion Mechanism," *IEEE/ASME Transactions on Mechatronics*, vol. 20, no. 6, pp. 2853-2861, Dec. 2015.

[3] L. Xie, S. Cai, G. Huang, L. Huang, J. Li and X. Li, "On Energy Harvesting From a Vehicle Damper," *IEEE/ASME Transactions on Mechatronics*, vol. 25, no. 1, pp. 108-117, Feb. 2020.

[4] F. Khoshnoud et al., "Energy Regeneration From Suspension Dynamic Modes and Self-Powered Actuation," *IEEE/ASME Transactions on Mechatronics*, vol. 20, no. 5, pp. 2513-2524, Oct. 2015.

[5] S. Guo, L. Xu, Y. Liu, X. Guo and L. Zuo, "Modeling and Experiments of a Hydraulic Electromagnetic Energy-Harvesting Shock Absorber," *IEEE/ASME Transactions on Mechatronics*, vol. 22, no. 6, pp. 2684-2694, Dec. 2017.

[6] X. Xia, D. Ning, Y. Liao, P. Liu, H. Du, W. Li and G. Liu, "Multi-objective Control Strategies of a Novel Multifunction Electrically Interconnected Suspension," *IEEE/ASME Transactions on Mechatronics*, vol. 28, no. 6, pp. 3339-3351, Dec. 2023.

[7] T. Suzuki, M. Mae, T. Takeuchi, H. Fujimoto and E. Katsuyama, "Model-based Filter Design for Triple Skyhook Control of In-Wheel Motor Vehicles for Ride Comfort," *IEEJ Journal of Industry Applications*, vol. 10, no. 3, pp. 310-316, 2021.

[8] N. Ochi, H. Fujimoto and Y. Hori, "Proposal of roll angle control method using positive and negative anti-dive force for electric vehicle with four in-wheel motors," in *2013 IEEE International Conference on Mechatronics (ICM)*, Vicenza, Italy, 2013.

[9] E. Katsuyama, M. Yamakado and M. Abe, "A state-of-the-art review: toward a novel vehicle dynamics control concept taking the driveline of electric vehicles into account as promising control actuators," *Vehicle System Dynamics*, vol. 59, no. 7, pp. 976-1025, 2021.

[10] H. Fujimoto, O. Shimizu, S. Nagai, T. Fujita, D. Gunji and Y. Ohmori, "Development of Wireless In-wheel Motors for Dynamic Charging: From 2nd to 3rd generation," in *2020 IEEE PELS Workshop on Emerging Technologies: Wireless Power Transfer (WoW)*, Seoul, Korea (South), 2020.

[11] M. Ito, T. Suto, A. Takahashi, T. Hara and R. Iwano, "Development of a High Power Density In-Wheel Motor Using Halbach Array Magnets," *IEEJ Journal of Industry Applications*, vol. 12, no. 6, pp. 1134-1140, 2023.

[12] T. Emmei and H. Fujimoto, "Force Control of In-Wheel-Motored Electric Vehicles," *IEEJ Journal of Industry Applications*, vol. 9, no. 4, pp. 284-291, 2020.

[13] H. B. Pacejka and E. Bakker, "The Magic formula tyre model," *Vehicle system dynamics*, vol. 21, no. S1, pp. 1-18, 1992.

[14] J. Dixon, "Suspension Geometry and Computation," New York, NY, USA:Wiley Online Library, 2009.

[15] H. Fujimoto and S. Harada, "Model-Based Range Extension Control System for Electric Vehicles With Front and Rear Driving-Braking Force Distributions," *IEEE Transactions on Industrial Electronics*, vol. 62, no. 5, pp. 3245-3254, May 2015.

[16] S. Morimoto, Y. Tong, Y. Takeda and T. Hirasa, "Loss Minimization Control of Permanent Magnet Synchronous Motor Drives," *IEEE Transactions on Industrial Electronics*, vol. 41, no. 5, pp. 511-517, Oct. 1994.

[17] T. Suzuki, F. Chauvicourt and H. Fujimoto, "High-Bandwidth Suspension Resonance Analysis of In-Wheel Motor Vehicle Using Multibody Dynamics," in *2021 IEEE International Conference on Mechatronics (ICM)*, Kashiwa, Japan, 2021.

[18] D. Karnopp, "Active damping in road vehicle suspension systems," *Vehicle System Dynamics*, vol. 12, no. 6, pp. 291-311, 1983.